

Published in final edited form as:

Nat Neurosci. 2017 January ; 20(1): 82–89. doi:10.1038/nn.4437.

Vibrissa motor cortex activity suppresses contralateral whisking behavior

Christian Laut Ebbesen^{1,2}, Guy Doron^{1,3}, Constanze Lenschow¹, and Michael Brecht¹

⁽¹⁾Bernstein Center for Computational Neuroscience Berlin, Humboldt-Universität zu Berlin, Berlin, Germany

⁽²⁾Berlin School of Mind and Brain, Humboldt-Universität zu Berlin, Berlin, Germany

Abstract

Anatomical, stimulation and lesion data implicate vibrissa motor cortex in whisker motor control. Work on motor cortex focused on movement generation, but correlations between vibrissa motor cortex activity and whisking are weak. The exact role of vibrissa motor cortex remains unknown. We recorded vibrissa motor cortex neurons during various forms of vibrissal touch, which were invariably associated with whisker protraction and movement. Free whisking, object palpation and social touch all resulted in decreased cortical activity. To understand this activity decrease, we performed juxtacellular recordings, nanostimulation and *in vivo* whole-cell-recordings. Social facial touch resulted in decreased spiking activity, decreased cell excitability and membrane hyperpolarization. Activation of vibrissa motor cortex by intra-cortical microstimulation elicited whisker retraction, as if to abort vibrissal touch. Various vibrissa motor cortex inactivation protocols resulted in contralateral protraction and increased whisker movements. These data collectively point to movement suppression as a prime function of vibrissa motor cortex activity.

Introduction

Vibrissa motor cortex (VMC, Fig 1a) is a cortical vibrissa representation originally identified by a variety of stimulation techniques^{1–8}. The huge size of this representation possibly reflects the great ecological relevance of vibrissa movements for rats^{9,10}. In contrast to classic studies on primate primary motor cortex (M1) activity^{11,12}, VMC activity is only weakly correlated with movement^{13–16}. It is not entirely clear why the correlation between whisker movement and VMC activity is weak, but we note that most of what we know about VMC activity during whisking comes from recordings in animals

Users may view, print, copy, and download text and data-mine the content in such documents, for the purposes of academic research, subject always to the full Conditions of use:http://www.nature.com/authors/editorial_policies/license.html#terms

Correspondence should be addressed to M.B. (michael.brecht@bccn-berlin.de).

⁽³⁾Current Address: NeuroCure Cluster of Excellence, Humboldt-Universität zu Berlin, Berlin, Germany

Author Contributions

C.L.E., G.D. and M.B. designed the study. C.L.E. performed tetrode experiments. C.L.E. and G.D. performed juxtacellular experiments. G.D. and C.L. performed whole-cell recordings. C.L.E. and G.D. performed microstimulation and blockade experiments. C.L.E. analyzed the data and performed statistical modeling. C.L.E. and M.B. wrote the first version of the manuscript. All authors assisted with analyzing data and contributed to writing the manuscript.

Competing Financial Interests

None.

simply whisking in air^{13–16}. Studies on primate motor cortex have shown, that besides the musculotopic representation of body movements^{17,18,12}, the motor cortex might also represent a map of ecologically relevant behaviors¹⁹. The information about VMC activity during self-initiated, ecologically relevant behaviors is still limited and it remains unclear how VMC contributes to motor control during such behaviors. This prompted us to pose the following questions about VMC function: (1) How is the activity of the VMC “output layers”⁸ modulated, when rats engage in various ecologically relevant whisking behaviors? (2) What are the cellular mechanisms, which contribute to the modulation of VMC activity? (3) How does an increase of VMC activity by microstimulation during whisking affect ongoing whisking movements? (4) How does a decrease of VMC activity by pharmacological blockade affect whisking movements?

Results

Vibrissa motor cortex firing decreases during various forms of vibrissal touch

We investigated VMC modulation by three self-initiated rat whisker behaviors (Fig. 1b): free whisking (explorative whisking bouts in air), object touch (whisking onto objects) and social touch (whisking onto conspecifics)²⁰. All whisker-behaviors were compared to rest (animal not whisking). Single unit activity was recorded from VMC layer 5 using tetrodes. With high-speed videography, we quantified the whisker set angle and whisking power during the various behaviors (Fig. 1c). We found that during all whisking behaviors the whiskers were held at a more protracted set angle than at rest, on average by 19° (Fig. 1d top, $P < 0.001$, one-way ANOVA, all $P < 0.001$, unpaired t-tests). By definition, during all whisking behaviors, the whisking power was higher than at rest (Fig. 1d bottom).

In Fig. 1e, we show a raster plot and a peri-stimulus time histogram (PSTH) of an example layer 5 cell aligned to the beginning of free whisking. The PSTH shows the predominant response pattern: a decrease in firing rate during free whisking. We observed a large variability of responses (Fig. 1e, top). Some cells increased their firing, some were not modulated and some decreased their firing rate, but as a whole the population activity was significantly decreased during free whisking (Fig. 1f top, median 2.31/2.05 Hz Baseline/free whisking, Slope = 0.812, $P = 0.00010$, $N = 158$ cells, Mann-Whitney U-test). We assessed the significance of firing rate changes by a bootstrapping procedure and found that 80% of significantly modulated cells decreased their activity in free whisking ($P = 0.000041$, two-tailed binomial test for equal proportions). We restricted our analysis to cells with a firing rate below 10 Hz to reduce the proportion of interneurons (see Methods). In the small subset of cells with firing rates > 10 Hz (14% of cells) we found no significant rate changes (All $P > 0.05$, Mann-Whitney U-test). Inclusion of high-firing cells did not change the results. To quantify the modulation of single cells, we calculated a modulation index (see Methods) and found that the most strongly modulated cells were the cells that decreased their firing rate (Fig. 1f bottom, $P < 0.05$, Mann-Whitney U-test). We wondered, if the firing rate decrease is also to be seen in more challenging forms of vibrissal touch. For both object touch (Fig. 1g,h top, median 2.20/1.65 Hz Baseline/Touch, Slope = 0.749, $P = 0.023$, $N = 122$ cells, Mann-Whitney U-test) and for social facial touch (Fig. 1i,j top, median 2.26/1.87 Hz Baseline/Touch, Slope = 0.806 $P = 0.00018$, $N = 156$ cells, Mann-Whitney U-test), neurons also

decreased their firing rate. Specifically, we observed a decrease in 88% of the cells significantly modulated by object touch (Fig. 1h bottom) and in 78% of the cells significantly modulated by social touch, (Fig. 1j bottom, both $P < 0.05$, two-tailed binomial tests). As during free whisking, the most strongly modulated cells were the cells that decreased their firing rate (Fig. 1h,j bottom, both $P < 0.05$, Mann-Whitney U-test).

Cellular mechanisms of vibrissa motor cortex suppression

Thus, the transition from rest (retracted whiskers, no movement) to whisker behaviors (protracted whiskers, whisking) leads to a decrease of VMC activity. In cortical physiology, this is a highly unusual result. In the somatosensory system and the visual system, relevant stimuli lead to an increase in population activity. To explore the cellular basis of the decrease of VMC activity during whisking, we habituated rats to head-fixation and performed juxtacellular recording, nanostimulation and whole-cell recordings from VMC putative layer 5 neurons, the output layer⁸. We focused on social touch, an engaging stimulus²¹, which strongly activates primary somatosensory cortex (S1)^{20,22} and medial prefrontal cortex²³. During recordings, we staged facial interactions of the head-fixed rats with stimulus rats in front of them (Fig. 2a). In agreement with the recordings in freely moving rats, we found that VMC activity strongly decreased during social facial touch episodes. As shown in Fig. 2b the rat protracted the whiskers during nose-to-nose touch and a juxtacellularly recorded neuron discharged fewer APs than at baseline. Across the population of neurons, we found a significant decrease of spiking during social facial touch compared to baseline (Fig 2c, median 2.5/2.0 Hz, baseline/social touch, $P = 0.0079$, $N = 21$ cells, Wilcoxon signed-rank test). To investigate if the decrease in spiking was due to a decrease in cell excitability, we evoked APs in single layer 5 neurons at baseline and during social touch episodes, using a nanostimulation protocol (Fig. 2d, see Methods). Across the population, we found that layer 5 neurons were indeed much less excitable during social facial touch than during baseline (Fig. 2e, median evoked rate 14.6/4.8 Hz, baseline/social touch, $P = 0.0125$, $N = 15$, Wilcoxon signed-rank test). To investigate the underlying intracellular signals, we targeted whole-cell patch-clamp recordings to the deep layers of VMC during social facial touch (Fig. 2f). In agreement with the reduced excitability, we found that the neurons were slightly but significantly more hyperpolarized during social facial touch than at baseline, on average by 1.5 mV (Fig. 2g, $P = 0.0171$, $N = 10$ cells, paired t-test). Some cells showed a reduction in the membrane potential coefficient of variation during social touch (e.g. Fig. 2f), but across the population, there was no significant change ($P > 0.05$, $N = 10$ cells, paired t-test). Both the dampening of spiking evoked by juxtacellular nanostimulation and the observed hyperpolarization point to increased somatic inhibition in VMC during whisker movement.

Whisker protraction and social touch drive suppression of vibrissa motor cortex

Even though social facial touch is generally associated with whisker movement and whisker protraction (Fig 1d), there is a large variability in the whisking between touch episodes^{20–22}. We decided to exploit this fact to disentangle whether the suppression of VMC activity during social facial touch (Fig. 2b) was due to the nose-to-nose touch, the coincidental whisker protraction and increased whisking amplitude, or perhaps a combination thereof. To this end, we juxtacellularly recorded an additional set of cells during social facial touch episodes, where we now also simultaneously recorded and tracked the whisker angle of the

contralateral whiskers using high-speed videography, using a robust method which captures most aspects of the whisker movements (Fig S1a-b, see Methods). We then used likelihood maximization to fit a Poisson model (with 1-ms bins) to the spike trains, where the instantaneous firing rate depends linearly on nose-to-nose touch (a binary variable), the whisker angle and the whisking amplitude by the coefficients β_{Nose} , β_{Angle} and β_{Ampl} (Fig. 3a-b, see Methods). After recording, we labeled and recovered cells, both Ctip2-positive cells (putative thick-tufted pyramidal tract (PT-type) neurons²⁴, Fig 3a-b) and Ctip2-negative cells (putative thin-tufted intratelencephalic (IT-type) neurons, example Fig. S1d-e). Across all cells, we found that the cells were suppressed by both nose touch (Fig. 3c, median $\beta_{Nose} = -0.60$, $P = 0.0067$, $N = 32$ cells, Wilcoxon signed-rank test) and by whisker protraction (Fig. 3c, median $\beta_{Angle} = -0.026$ ($^{\circ}$)⁻¹, $P = 0.020$, $N = 32$ cells, Wilcoxon signed-rank test). We did not find a systematic dependence on the whisking amplitude across the population (median $\beta_{Ampl} = -0.026$ ($^{\circ}$)⁻¹, $P > 0.05$, $N = 32$ cells, Wilcoxon signed-rank test). When we used a likelihood ratio test to select single cells, which were significantly modulated by amplitude (at $P < 0.05$, see Methods), the results were also mixed (Fig S1c): 10 cells were significantly suppressed, 6 cells were significantly activated, and 16 cells were not significantly modulated. However, we note suppressed cells were more strongly modulated than the activated cells: (median $|\beta_{Ampl}| = 0.221/0.128$ for suppressed/activated cells, $P = 0.00025$, Mann-Whitney U-test). In our subset of labeled cells, we did not find indications, that PT or IT type cells had different response patterns; both cell types were generally suppressed by nose touch and whisker protraction (data not shown). To control for possible collinearity, we also fitted a model, where we performed stepwise orthogonalization of the predictor vectors ‘nose touch’, ‘angle’ and ‘amplitude’ using the Gram-Schmidt algorithm. In this case, we found the same pattern: the β_{Nose} ’s and the β_{Angle} ’s were significantly negative (Fig. S1f)

Since each cell is associated with an individual estimate of the baseline firing rate and dependence on nose touch and whisker protraction, we could evaluate our model for all cells to estimate the population activity during various whisker behaviors. We first compared the baseline firing rate ($\lambda_{rest} = \exp(\beta_0)$) to the firing rate during nose touch ($\lambda_{touch} = \exp(\beta_0 + \beta_{Nose})$). In agreement with Fig. 2c, we found that the population activity is suppressed during nose touch (Fig 3d, median 1.69/1.15 Hz, baseline/nose touch, $P = 0.036$, $N = 32$ cells, paired t-test), even in the absence of whisker protraction. Similarly, when we calculated the modulation index resulting from comparing rest to nose touch (Fig 3e, left, median index: -0.29 , $P = 0.0067$, $N = 32$ cells, Wilcoxon signed-rank test), comparing rest to 15° whisker protraction (Fig 3e, middle, median index: -0.19 , $P = 0.020$, $N = 32$ cells, Wilcoxon signed-rank test) and from comparing rest to nose touch coinciding with 15° whisker protraction (Fig 3e, right, median index: -0.40 , $P = 0.00041$, $N = 32$ cells, Wilcoxon signed-rank test), we found that all conditions lead to a suppression of the population activity. We conclude, that the suppression of activity during exploratory whisking in air and during social facial touch, which we observe in behaving animals (Fig 1 & 2), likely results from a suppression due to both nose touch and coincidental whisker protraction (Fig 3c).

Activation of vibrissa motor cortex by microstimulation

In order to better understand the role of VMC activity in control of contralateral movement during ongoing whisking, we decided to test the effect of increasing VMC activity by intracortical microstimulation at a behavioral time scale in the range where we observed modulation of VMC activity¹⁹. To this end, we unilaterally microstimulated VMC deep layer cells during bouts of free whisking using 1 s long stimulation pulse trains randomly preceded or followed by a 1 s long break (“sham stimulation”) (Fig. 4a, see Methods). The dominant effect of such stimulation was the retraction of the contralateral whiskers (Fig. 4b, $1.2 \pm 0.7^\circ/\text{s}$ vs. $-2.4 \pm 1.5^\circ/\text{s}$, sham vs. stimulation, $P = 0.0000245$, paired t-test). We also observed a small increase in the contralateral whisking power during the stimulation pulses, suggesting that we induced extra movement of the contralateral whiskers (11% increase, Fig. 4c, $194 \pm 64(^\circ)^2$ vs. $216 \pm 64(^\circ)^2$, $P = 0.0151$, paired t-test). We wondered, if the extra induced backwards movement might be enough to influence social touch behavior, so we also performed a set of experiments, where we unilaterally microstimulated VMC deep layers during social facial touch episodes. When comparing the duration of social facial touch episodes from first to last whisker touch, we found that microstimulation significantly shortens the whisker touches (Figure S2, mean duration 0.692/0.973 s, stimulation/sham, $P = 0.0000011$, LME model), consistent with the finding that VMC activation induces whisker retraction to abort social facial touch.

Blockade of vibrissa motor cortex

We wondered, how whisking would be affected by VMC inactivation and therefore pharmacologically blocked VMC deep layer activity unilaterally by injection of lidocaine. As shown in an example experiment prior to lidocaine injection, the rat’s whiskers were positioned symmetrically (Fig. 5a left). After lidocaine injection, the whiskers were asymmetric and more protracted contralaterally (Fig. 5a right). Similarly, the rat whisked with equal whisking amplitude ipsilaterally and contralaterally prior to lidocaine injection (Fig. 5b, left), but whisked with much larger amplitude on the contralateral side than on the ipsilateral side after blockade (Fig. 5b right). The same observations were made across a series of experiments. Injection of lidocaine solution (Fig. 5c left, $P = 0.0052$, $N = 10$, paired t-test) but not of ringer solution (Fig. 5c right) led to a significant increase in the contralateral whisking power. Similarly, injection of lidocaine but not of ringer solution led to a protraction of the contralateral whiskers by an average of 21° (Fig. 5d, $-7.0 \pm 16.3^\circ$ vs. $14.2 \pm 7.3^\circ$, $P = 0.0012$, $N = 10$, paired t-test). Neither injection of ringer nor lidocaine had an effect on the set angle of the ipsilateral whiskers. When we unilaterally blocked excitatory currents in the VMC by superfusion of APV (an NMDA antagonist) and NBQX (an AMPA antagonist) in lightly anaesthetized rats (Figure S3, $N = 3$ rats), and when we blocked VMC activity by injection of muscimol (a GABA_A agonist) in lightly anaesthetized mice (Figure S4, $N = 4$ mice), we saw the same effects: protraction of contralateral whiskers and increased contralateral whisker movements.

Discussion

Summary

Most work on the mammalian motor cortex has focused on a role of this cortical area in movement generation^{11,12}. It is therefore surprising that our observations coherently indicate that a prime function of VMC activity might be to suppress behavior: *(i)* When the rat engages in whisker-related behavior (protracted whiskers, whisker movements), we see a decrease in spiking activity in the VMC output layers (Fig. 1-3). *(ii)* VMC microstimulation leads to retractive movements, as if to abort behavior (Fig. 4). *(iii)* VMC blockade disinhibits contralateral whisker movements and leads to contralateral whisker protraction, as if to engage in behavior (Fig. 5). Our observations are difficult to reconcile with the classic model, where the prime role of VMC activity is whisker protraction and the generation of movement⁷. Instead the data support a model where VMC activity suppresses whisker behavior, perhaps by gating a downstream whisking central pattern generator^{6,14,25,26}.

Relation to previous vibrissa motor cortex studies

The whisker motor plant^{27,28} and vibrissa motor neurons²⁹ are laid out for the fine control of individual whisker protraction. This is in line with a prime function of vibrissal touch in palpation of objects, obstacles and conspecifics in front of the animal^{9,10}. In light of the specialization of the motor plant and motor neurons for whisker protraction, our observation that VMC deep layer microstimulation leads to whisker retraction is quite surprising. This retraction result is in agreement with previous studies, which have all reported that VMC microstimulation^{1–5}, single-cell stimulation⁶ and optogenetic stimulation⁷ elicit with few exceptions^{3,7} whisker retraction. The retraction movements let it appear unlikely that an increase in VMC activity drives vibrissal touch (which is associated with whisker protraction, Fig. 1d). Rather, it suggests, that the role of VMC is to abort undesired whisking behavior. This idea is also supported by the unexpected increase of contralateral whisking following acute VMC blockade. Our observation that a reduction in motor cortex activity increases movement is consistent with observations on whisking patterns after VMC lesions: Whisking persists after VMC ablation⁹ and blockade^{7,30}, VMC ablation spares large-amplitude whisking, but reduces small whisker movements³¹, and unilateral VMC lesions increases contralateral whisking power³².

While the bulk of our data point to motor suppressive effects of VMC activity, some of our results also point to a role of VMC cells in movement generation. Thus, a small subset of VMC cells weakly increased their firing rate during movements (Fig 1-2). Further, generalized linear modeling of VMC activity revealed, that the relationship between VMC activity and whisking amplitude was mixed with no obvious pattern (Fig 3). This is consistent with previous studies, which have reported both negative and positive correlations between activity of single VMC cells and whisking power^{13–16}. A novelty of our study is that we used statistical modeling to analyze all spikes and relate them to naturalistic behavior (whisker angle, amplitude and social touch episodes), i.e. we did not only analyze whisking in air^{13–16} and we did not exclude periods, where the amplitude was low¹⁴ (breaks in whisking are also a part of natural whisking patterns). Speaking more generally,

movement suppression and movement generation are probably inseparable aspects of motor control.

Is the functional output of vibrissa motor cortex a decrease in spikes to downstream targets?

The output of vibrissa motor cortex is thought to play two major roles: First, it is supposed to control whisker movement, presumably by gating a downstream whisking central pattern generator in the brainstem (PT-type neurons)^{14,25,26}. Secondly, it is supposed to transmit an efferent, internal signal to sensory cortices, so they can disentangle afferent sensory signals due to touch stimulation of the whiskers from sensory signals due to self-generated whisker movement (IT-type neurons)¹⁰. Previous investigations of the relationship between VMC activity and whisking have found that the overall modulation of VMC activity due to whisking is weak, although single cells exist which correlate with the whisking amplitude^{13–16} and the whisker angle¹⁴. These single cells have previously been found in roughly equal proportions, and it has remained unclear what the prime ‘functional’ output of the VMC might be^{14,16}.

In neurophysiology we normally observe that cells respond to behavior with an increase of activity. This is the case in the somatosensory system and the visual system, and has been proposed to be a governing principle for cortical information processing. Thus, our observation that the ‘functional’ response of VMC cells during various whisker behaviors is a *decrease* in spiking is highly surprising. The whisker motor plant is laid out for controlled forward movement, yet we found that VMC activity decreases with whisker protraction (Fig. 1,3). Social facial touch is a very engaging stimulus, where correct sensorimotor computation is of high ecological importance²¹, yet we robustly see a decrease in VMC activity and a decrease in VMC excitability during social touch episodes (Fig 1-3). For comparison, previous studies have found that social facial touch very strongly activates primary somatosensory cortex (S1)^{20,22} and medial prefrontal cortex²³. Cells, where the functional response is a hyperpolarization, are rare but not unknown (e.g. the photoreceptor of the mammalian eye), yet our findings are very unusual for a primary cortical area.

Motor suppressive effects of motor cortex

Motor effects of motor cortex lesions in rats are subtle, as many simple behaviors (e.g. locomotion) persist after decortication³³. Motor cortex lesions are associated with performance deficits in several movement related tasks, but at least some of these deficits are not primarily due to deficits in the generation of movement, but to deficits in the control and suppression of movement³³. For instance, rats can perform long sequences of skilled, learned motor behaviors after motor cortex ablation, but motor cortex is required for them to learn a task of behavioral inhibition (they must learn to postpone lever presses)³⁴. When swimming, intact rats hold their forelimbs still and swim with only their hindlimbs. After forelimb motor cortex lesions, however, rats swim with their forelimbs also³⁵. After learning a go/no-go whisker task, where mice must lick to receive a water reward, motor cortex inactivation does not significantly decrease the licking at correct times, but massively increases the ‘false alarm’ licking rate (where licking should be suppressed)^{30,36}. Human patients with frontal lesions are notorious for their lack of behavioral control and do things,

they should not do³³, rodents with lesions in motor cortex often perform movements, that should rather be suppressed.

Motor-suppressive effects are impossible to detect in classic motor mapping experiments in lightly anaesthetized animals^{1–6,8,37}, but human patients report an inability to move as a prominent effect of intra-operative stimulation of motor cortex^{18,38,39}. The existence of these negative motor areas (NMAs) in M1 where stimulation elicit an inhibition of movement is a robust result, but even in humans there has historically been a strong bias towards the study of positive motor effects of M1 stimulation, and consequently the function of NMAs in the inhibitory control of movement is still poorly understood³⁹. Furthermore, a complication is that NMA stimulation can elicit positive movements with an increasing stimulation current³⁸, and may as such simply be missed, if only positive stimulation effects are evaluated³⁹.

Is rat vibrissa motor cortex different from primate motor cortex?

Our observation that a decrease in VMC activity leads to whisker protraction is incompatible with a model where VMC PT-type neurons synapse directly onto whisker motor neurons in the facial nucleus. This direct wiring pattern from motor cortex to motor neurons is famously present in primate hand motor cortex⁴⁰, where overwhelming evidence suggests, that in contrast to our observations of rat VMC, activity mainly correlates positively with movement^{11,12}. Indeed, there is only a very sparse direct projection from VMC to the whisker motor neurons⁴¹ with the vast majority of VMC PT-type neurons targeting brainstem interneurons⁴².

It is worth noting, that even in primates, the predominant wiring pattern of corticobulbar and corticospinal projections from M1 is to brainstem and spinal interneurons⁴⁰. The monosynaptic projections from M1 to motor neurons innervating distal limb muscles is an exception, which evolved in primates in parallel with the evolution of skilled digit movements⁴⁰. Spike-triggered averaging techniques used in monkeys have all showed that M1 neuron spikes can predict both EMG peaks and troughs, which suggest that M1 neurons commonly have suppressive effects on motoneuronal pools^{12,43,44}. Recent single-cell recordings in monkeys have shown, that also in primates, some M1 cells correlate negatively with movement: Both premotor neurons⁴⁵ and indeed M1⁴⁶ and M1 pyramidal tract neurons^{47,48} respond with mirror neuron activity to the observation of actions, even when the monkey is not moving, a kind of “monkey see, monkey *not* do” response⁴⁹. Similarly, although some muscle weakness is a symptom in patients with M1 or pyramidal tract lesions, the prominent symptoms are ataxia (loss of control over movements), spasticity, clonus, hyperexcitability of reflexes⁵⁰. Spastic paralysis can be managed by high doses of muscle relaxants to reduce the output from the spinal cord or by sectioning the dorsal roots, suggesting that it represents an abnormal increase in muscular input from the spinal cord due to a net loss of descending inhibition from M1⁵⁰.

Conclusion

Action suppression is vital for behavior and numerous studies point to a frontal cortical location of this important cognitive capacity³³. Our observations suggest that the classic

work on the role of motor cortex in movement generation should be complemented by a more extensive investigation of motor suppressive functions of motor cortices.

Online Methods

Animal welfare

All experimental procedures were performed according to German animal welfare law under the supervision of local ethics committees. Rats (Wistar) and mice (C57BL/6) were purchased from Janvier Labs (Le Genest-Saint-Isle, France). Stimulus animals were housed socially in same-sex cages, and post-surgery implanted animals were housed in single animal cages. All animals were kept on a 12h:12h reversed light/dark cycle and all experiments were performed in the animals' dark phase. Rats had ad libitum access to food and water.

Whisking behavior

Behavioral experiments were done using the social gap paradigm^{20,21,51} (Fig 1b). The experimental paradigm consists of two elevated platforms, 30 cm long and 25 cm wide surrounded by walls on 3 sides, positioned approximately 20 cm apart. The distance between platforms was varied slightly depending on the size of the rats. The platforms and platform walls were covered with soft black foam mats to provide a dark and nonreflective background and to reduce mechanical artifacts in tetrode recordings. All experiments were performed in darkness or in dim light, and behavior was recorded from above under infrared light. The implanted rat was placed on one platform, and on the other platform we either presented various objects or other rats. The implanted rats were not trained, just habituated to the setup and room and spontaneously engage in investigation of the objects or social facial interactions.

The rat behavior was recorded at low speed from above with a 25 Hz digital camera, synchronized to the electrophysiological data acquisition using TTL pulses to trigger each frame. Additional 250 Hz high-speed recordings were performed, when the rats were freely whisking over the gap, socially interacting or investigating objects. Typically, recording sessions were performed in four to eight 15 min blocks, where we would present either objects or conspecifics (of both sexes) in each block, randomly. The video frames of the 25 Hz videos were labelled in four categories: "Free whisking" (Animal freely whisking into air), "Object touch" (animal touching an object with its nose), "Social touch" (animal touching a conspecific nose-to-nose) and "Rest" (animal not whisking). Videos were labeled blind to the spike data.

In our assessment of the whisker set angle and whisker power during the various whisker behaviors, we included a large dataset of already-tracked whisker traces, some of which have previously been published by Bobrov et al.²⁰ and Rao et al.⁵¹.

To quantify the whisking behavior, the whisker traces were tracked from the 250 Hz video frames, as previously described^{20,21,51}. We band-pass filtered the raw tracked whisker trace to remove jitter due to the tracking (2nd order Butterworth filter from 0.25 to 12.5 Hz). The whisking power was calculated from a spectrogram constructed by performing a

Stockwell transform⁵² from 0-20 Hz (frequency steps of 0.1 Hz), and by integrating the absolute value of the power spectral density in the 0-20 Hz band over time to calculate an average power. The set angle was estimated by calculating the average angle of the whisker trace.

Tetrode recordings

In tetrode recording experiments, we used p60 Wistar rats (3 male, 2 female), which were handled for 2-3 days, before being implanted with a tetrode microdrive over the vibrissa motor cortex. Surgery was done as previously described²⁰. The implanted microdrive had eight separately movable tetrodes driven by screw microdrives (Harlan 8-drive; Neuralynx, Bozeman, MT, USA). The tetrodes were twisted from 12.5 μm diameter nichrome wire coated with polyimide (California Fine Wire Company), cut and examined for quality using light microscopy and gold-plated to a resistance of ca. 300 k Ω in the gold-plating solution using an automatic plating protocol (“nanoZ”, Neuralynx). For tetrode recordings, a craniotomy of 1x2 mm was made 0.75-2.75 mm anterior and 1-2 mm lateral to bregma, corresponding to the coordinates of VMC5. Steel screws for stability and two gold screws for grounding the headstage PCB were drilled and inserted into the skull, and the gold screws were soldered and connected to the headstage PCB using silver wire. After fixation of all screws, the dura was removed, the implant fixated in the craniotomy, the craniotomy sealed with 0.5% agarose and the tetrode drive fixed in place with dental cement (Heraeus). The tetrodes were arranged in a 2-by-4 grid ($d \approx 500 \mu\text{m}$). Neural signals were recorded through a unity-gain headstage preamp and transmitted via a soft tether cable to a digital amplifier and A/D converter (Digital Lynx SX; Neuralynx) at 32 kHz. We filtered the signal between 600 Hz and 6 kHz and detected spikes by crossing of a threshold (typically $\sim 50 \mu\text{V}$) and saved each spike (23 samples - 250 μs before voltage peak and 750 μs after voltage peak). At the end of the experiment, animals were again anaesthetized with a mix of ketamine and xylazine, and the single tetrode tracks were labelled using small electrolytic lesions made by injecting current through the tetrode wire (10 μA for 10 s, tip-negative DC). After lesioning, animals were perfused with phosphate buffer followed by a 4% paraformaldehyde solution (PFA). Brains were stored overnight in 4% PFA before preparing 150 μm coronal sections. Sections were stained for cytochrome oxidase to reveal the areal and laminar location of tetrode recording sites, which could be calculated from the location of tetrode tracks and lesions. We only analyzed data from recording sites, where the lesion pattern could unanimously identify the tetrode and the recording sites.

All spike analysis was done in Matlab (MathWorks, Natick, MA, USA). Spikes were preclustered off-line on the basis of their amplitude and principal components by means of a semiautomatic clustering algorithm (KlustaKwik by K. D. Harris, Rutgers University). After preclustering, the cluster quality was assessed and the clustering refined manually using MClust (A. D. Redish, University of Minnesota). The spike features used for clustering were energy and the first principle component of the waveform. To be included in the analysis as a single unit, clusters had to fulfill the following criteria: first, the L-ratio, a measure of distance between clusters⁵³, was below 0.5. Second, the histogram of inter-spike intervals (ISIs) had to have a shape indicating the presence of single units, e.g. a refractory time of

1-2 ms, or the appearance of a bursty cell (many short ISIs). Multi-unit clusters were not included in the analysis.

Since we wanted to investigate the contribution of VMC to motor control, we were interested in the spiking activity of the pyramidal projection neurons in layer 58. Due to the different morphology and ion channel populations in the cell membrane, interneurons and pyramidal cells can sometimes be separated based on the shape of the extracellular spike waveform⁵⁴. We tried various combinations of spike shape parameters such as spike-width, peak-to-trough time, shape of after-hyperpolarization, but none yielded convincingly bimodal distributions which allowed separation of cells into regular-spiking putative pyramids and fast-spiking putative interneurons (data not shown). This may relate to the fact that motor cortex projection neurons actually have exceedingly narrow spikes⁵⁵. Since separation by spike shape was not feasible, we instead reduced the proportion of fast-spiking interneurons in our sample by simply excluding very-high firing cells (mean rate during whole recording session above 10 Hz) from the analysis.

To assess, if single cells were significantly modulated by whisker behaviors, we used a bootstrap method: First, we calculated a modulation index: $Idx = (R_{\text{behavior}} - R_{\text{baseline}}) / (R_{\text{behavior}} + R_{\text{baseline}})$ where R_{behavior} and R_{baseline} is the average firing rate at baseline and during the behavior (e.g. during social touch), respectively. In the bootstrapping, we avoided bias by having a balanced baseline design, where the baseline was defined to be segments of time of equal lengths to the nose-to-nose touches, just prior to the beginning of nose-to-nose touches. We generated a distribution of 10,000 bootstrapped dummy modulation indices by preserving the lengths of the nose-to-nose touches, but randomly placing the start-times within the recordings. If the real modulation index was below the 2.5th or above the 97.5th percentile of the bootstrapped dummy indices (i.e. a two-tailed test at $\alpha = 0.05$), the cell was taken to be significantly modulated. After having assessed that a cell was significantly modulated, we compared significantly modulated cells to "Rest". Here we calculated a similar modulation index: $\text{Modulation index} = (R_{\text{behavior}} - R_{\text{rest}}) / (R_{\text{behavior}} + R_{\text{rest}})$, where R_{behavior} and R_{rest} is the average firing rate. The response index is symmetric and can take on values between -1 (cell only spikes at "Rest") and +1 (cell only spikes during behavior). To compare the modulation strength of suppressed and increased cells, we compared the absolute value of this response index.

Juxtacellular and whole-cell recordings

In juxtacellular recording experiments, rats were between 30 and 40 days old, males and females. Whole cell patch clamp recordings were made in younger animals, aged between P25-P30 at the day of the final experiments. Rats were handled for 2-3 days, before being implanted with a head-fixation post and were habituated until the rat was comfortable with head-fixation for 60 minutes, as previously described²². After the habituation procedure a second surgery was performed, during which a craniotomy was drilled over the vibrissa motor cortex (1.5 mm anterior, 1.5 mm lateral from bregma) and a recording chamber was implanted. In the case of patch-clamp recordings the dura was removed using a bent syringe. The preparation was covered with silicone (Kwik-Cast, World Precision Instruments). After

the second surgery, the animals recovered (for at least half a day) before the recording sessions started.

Juxtacellular and whole-cell patch-clamp recordings were made using glass electrodes made of borosilicate glass tubes (Hilgenberg) pulled to have a resistance of 4 to 7 M Ω . For whole-cell, pipettes were lowered into the cortex with positive pressure (200-300bar). For whole-cell recordings and for juxtacellular experiments shown in Fig. 2, the pipettes was filled with intracellular solution of 135 mM K-gluconate; 10 mM HEPES; 10 mM Na₂-phosphocreatine; 4 mM KCl; 4 mM MgATP; and 0.3 mM Na₃GTP (pH 7.2). After the pipette reached 150-200 μ m below the surface the following steps were different depending on the recording type. For juxtacellular recordings a search current step was applied and the pipette was lowered stepwise through the cortex (step size: 3 μ m) until a cell could be detected by excitability (as previously described⁵⁶). In the case of patched cells, the positive pressure in the pipette was lowered to 30 bars to search for cells and the pipette was lowered with a step size of 3 μ m through the cortex. When the pipette resistance increased, suction was applied to establish a gigaohm seal and achieve the whole-cell configuration. The recorded signal was amplified by a patch-clamp amplifier (Dagan) and sampled at 25 kHz by a Power1401 data acquisition interface under the control of Spike2 software (CED). All head-fixed recording and stimulation experiments were performed at a depth reading of $1423 \pm 512 \mu\text{m}$ (mean \pm SD) from the pia, corresponding to putative layer 5 of VMC. We did not record fast-spiking putative interneurons and only regular spiking, putative pyramidal neurons were included in the analysis.

For juxtacellular recordings shown in Figure 3, the pipette was filled with Ringer's solution and 1-1.5 % biocytin or Neurobiotin (VectorLabs) with pH = 7.2 (adjusted by adding NaOH) and final osmolality ~ 290 mmol/kg. After experiments, the recorded neuron was labeled by a Pinault protocol⁵⁷. The rat was perfused, the brain was sectioned coronally (60 μ m sections) and the labeled cell was visualized by staining with Streptavidin conjugated to Alexa Fluor 546 (Life Technologies, 1:1000) as previously described⁵⁸. Ctip-2-positive (putative PT-type cells²⁴), were labeled by an Anti-Ctip2 antibody (Abcam 25B6, ab18465, 1:1000) visualized by staining with Alexa Flour 546 (1:1000) as described by Sürlemlı et al. ⁵⁹.

During head-fixed recording sessions, stimulus rats, hand held by the experimenter, were presented in front of the head-fixed rat the rats were allowed to socially interact²² (Figure 2a). To monitor social interactions, 25 Hz and 250 Hz digital video synchronized to the electrophysiology data was recorded from above by triggering frames and recording from a Spike2 script. The whisker movements were tracked from the 250 Hz videos using a custom written computer software for whisker tracking (Viktor Bahr, adapted from Clack et al. 2012⁶⁰). Behavioral events (beginning and end of nose touches) were labeled in the 25 Hz videos. All video analysis was performed blind to the electrophysiology data.

To estimate the firing rate change during social facial touch in the head-fixed animals, we computed the average firing rate during 1 s preceding start of social facial touch (beginning of nose-to-nose touch), this we used as a baseline firing rate. Firing rates during social facial touch were computed by averaging the firing rate in a 1 s response window after the onset of

nose-to-nose touch. In this analysis, we included both juxtacellularly recorded cells, and patched cells which were spiking. To estimate the change in cell excitability, we calculated the average firing rate from juxtacellularly nano-stimulated cells during positive stimulation pulses (typically ~2 nA, adjusted per cell), where the rat was not engaging in social facial touch (the baseline). This we compared to the average firing rate during stimulation pulses that happened during a social facial episode (i.e. while the rats were touching nose-to-nose). To estimate the hyperpolarization of the patched cells during social facial touch episodes, we clipped the spikes from the membrane potential and compared the average membrane potential during social facial touch episodes to the average membrane potential during 1 second preceding start of social facial touch (the baseline).

Automatic whisker tracking in socially interacting, head-fixed animals

We used a correlation-based algorithm to automatically track the whisking during juxtacellular recordings in head-fixed rats: We filmed the rats from above using a high-speed camera (250 frames/s, Figure 1b). For each tracked video, we manually clicked a pivot point on the center of the whisker pad and drew a tracking region of interest (ROI) around the whiskers contralateral to the recording craniotomy (Fig S1a). To estimate the change in mean whisker angle ('Angle') between two adjacent video frames, we calculated the correlation between the two frames within the tracking ROI (Pearson's ρ calculated between the greyscale values of the pixels) and rotated the previous frame around the pivot point (with nearest-neighbor interpolation), so that the correlation was maximized. This method was very robust, since it considers many whiskers simultaneously, and also worked during nose-to-nose touch episodes, where a few whiskers of the stimulus rat might enter the tracking ROI (Figure S1b, middle). Artifacts from badly tracked video frames were detected as sudden spikes in the correlation (Figure S1b, top) and the corresponding estimated values of Angle were removed (by a threshold, we used $\rho > 0.03$). To estimate the mean whisker angle ('Angle', Figure S1b, bottom), we linearly interpolated, numerically integrated and bandpass filtered Angle. For filtering, we used a bandpass IIR filter from 5-15 Hz in Matlab, to remove low-frequency drift stemming from the discrete integration. Since our tracking method considers all whiskers within the whisking ROI, our calculated whisker angle should be thought of as the mean deviation from the mean set angle of the whiskers, i.e. Angle = 10° corresponds to a mean-field, net 10° degrees whisker protraction, not an absolute whisker angle of 10°.

Maximum likelihood modeling

We used maximum likelihood modeling to estimate the dependence of VMC activity on the three covariates nose-to-nose touch, whisker angle and whisking amplitude, by fitting a Poisson model to the spike trains⁶¹. First, we binned the spike train in 1 ms bins. We assume, that the discharge of spikes within one time bin is generated by a homogenous Poisson point process, so that the probability of observing y spikes in a time bin is:

$$p(y | \lambda) = \frac{(\lambda \Delta)^y}{y!} \exp(-\lambda \Delta)$$

Where $\Delta = 1$ ms is the width of the time bin and $\lambda > 0$ s⁻¹ is the expected discharge rate of the cell. If we assume, that each time bin is independent, the probability of the entire spike train, \bar{y} is:

$$p(\bar{y}|\bar{\lambda}) = \prod_i \frac{(\lambda_i \Delta)^{y_i}}{y_i!} \exp(-\lambda_i \Delta)$$

where y_i, λ_i is the observed number of spikes and the expected discharge rate in the i 'th time bin, respectively. If we model the expected discharge rate, $\bar{\lambda}$, so that it depends on some parameters, $\bar{\beta}$, we have the log-likelihood function:

$$\mathcal{L}(\bar{\beta}) = \log p(\bar{y}|\bar{\lambda}(\bar{\beta})) = \sum_i y_i \log \lambda_i + \sum_i y_i \log \Delta - \sum_i \log y_i! - \Delta \sum_i \lambda_i$$

For our purpose, we model $\bar{\lambda}$ so that it depends on the spike history and linearly on a 1-ms interpolated vector indicating nose touch, \overline{Nose} (either 0 or 1), a vector of the whisker angle, \overline{Angle} , and a vector of the whisking amplitude, \overline{Ampl} (calculated by quadratically splining the local maxima of the rectified whisker angle). Due to the refractory period of the cell, it is not correct to assume, that all time bins are statistically independent, so following MacDonald et al. 201161, we also include 11 spike history parameters, $h_1 \dots h_{11}$, to model the interspike interval distribution of the cell. The spike history term is binned to 11 successive bins, five 1-ms bins (vectors $\bar{n}_1 \dots \bar{n}_5$: no. of spikes in the previous 0-1 ms, 1-2 ms, 2-3 ms, 3-4 ms, 4-5 ms,) and six 25-ms bins (vectors $\bar{n}_6 \dots \bar{n}_{11}$: no. of spikes in the previous 5-30 ms, 30-55 ms, 55-80 ms, 80-105 ms, 105-130 ms, 130-155 ms). We thus have:

$$\lambda_i = \exp(\beta_0 + \beta_{Angle} \cdot Angle_i + \beta_{Ampl} \cdot Ampl_i + \beta_{Nose} \cdot Nose_i + \sum_{j=1}^5 h_j \cdot n_{i,j}^{1msbin} + \sum_{j=6}^{11} h_j \cdot n_{i,j}^{25msbin})$$

For each cell, we fit the model by adjusting the parameters $\beta_0, \beta_{Angle}, \beta_{Ampl}, \beta_{Nose}, h_1 \dots h_{11}$ so that we maximize the log-likelihood function (using 'fminunc' in Matlab).

Since we did not find a dependence of the population activity on whisking amplitude, we also fitted a reduced model to the spike train, which does not depend on the whisking amplitude:

$$\lambda_i^{reduced} = \exp(\beta_0 + \beta_{Angle} \cdot Angle_i + \beta_{Nose} \cdot Nose_i + \sum_{j=1}^5 h_j \cdot n_{i,j}^{1msbin} + \sum_{j=6}^{11} h_j \cdot n_{i,j}^{25msbin})$$

We then used a likelihood ratio test between the full model and the reduced model to estimate if single cells are significantly modulated by the whisking amplitude. Since there is one less fitted parameter in the reduced model, the log-likelihood ratio:

$$LLRT = -2\log\left(\frac{\text{likelihood of simpler model}}{\text{likelihood of model with additional terms}}\right) \\ = 2(\mathcal{L}^{\text{full}} - \mathcal{L}^{\text{reduced}})$$

follows a χ^2 -distribution with one degree of freedom ($\nu = 1$). The p-value of the increase in likelihood due to including whisking amplitude in the model can thus be evaluated using the 'chi2cdf' function in Matlab. We classified cells with $p < 0.05$ as significantly modulated (Figure S1c).

Intra-cortical microstimulation

Animals were surgically prepared and habituated to head-fixation as described above. The microstimulation⁶² was done with 0.3 ms, 50 μ A unipolar negative-tip current pulses at 100 Hz through a tungsten microelectrode in deep layers (putative layer 5) of the VMC (depth = 1500 μ m from the dura). Current pulses were delivered from a stimulus isolator (World precision instruments, Sarasota, USA), gated by TTL pulses sent from a CED Power1401 by protocols written in Spike2 (Cambridge Electronic Design, Cambridge). The stimulation paradigm was blocks of 1 s long stimulation trains interspersed with 1 s long pauses in stimulation ("sham stimulation"). We observed the rats, and when the rats were whisking, we performed the microstimulation protocol during the ongoing whisking. A random number generator ensured that the stimulation would either start with stimulation or with sham stimulation, as not to bias the experiment. Synchronized 250 Hz digital high-speed video was recorded by triggering frames and recording from a Spike2 script. The whisker movements were tracked using a custom written computer software for whisker tracking (Viktor Bahr, adapted from Clack et al. 2012). Whisker tracking was done blind to the timing of stimulation and sham stimulation.

To quantify the change in whisking power due to microstimulation, we filtered the trace to remove jitter and calculated the whisking power as described above. To quantify the change in whisker set angle during the 1 s stimulation periods, and 1 s sham periods, we fitted straight lines to the whisker trace during each 1 s period. We took the slope of these straight lines to be a measure of the average change of whisker set angle per time ($^{\circ}$ /s), and averaged across these slopes for each experimental session.

For microstimulation in awake, socially interacting rats in the social gap paradigm, we used the same microstimulation train as in head-fixed animals, but the microstimulation was applied to deep layer VMC through the tetrode wires, implanted for recording (see above). Stimulation sites were confirmed post-hoc by histology. In these experiments, the stimulation was triggered by the experimenter (who was watching the infrared video) whenever the rats started socially interacting. The duration of social facial touch was quantified from the 25 frames/s video from the first to last whisker touch of the implanted rat. Since we had a varying number of data points per rat (depending on how many days the

stimulation sites were found to be in VMC layer 5), we compared the differences between median social facial interaction duration between the stimulated and sham stimulated days by fitting a linear mixed effects model (LME model) assuming a gaussian error distribution, with a random rat-specific intercept ('Length ~isStim + (1| Rat)') to account for mean differences among rats⁶³.

Vibrissa motor cortex blockade in awake rats

Animals were surgically prepared and habituated to head-fixation as described above. Borosilicate injection pipettes (Hirschmann Laborgeräte, Eberstadt, Germany) were pulled to a sharp tip and backfilled with Ringer or a 2% lidocaine solution⁶⁴ (bela-pharm, Vechta, Germany). 250 nL Lidocaine was slowly pressure-injected into deep layers (putative layer 5) of the VMC (depth = 1500 μm from the dura) at two injection sites: (1.75 mm anterior, 1.5 mm lateral to bregma) and (1.25 mm anterior, 1.5 mm lateral to bregma), ~2-5 min pr. injection. Based on measurements on the spatial spread of injection of 2% lidocaine in cortex⁶⁴, we estimate that the injection of 250 nL lidocaine inactivated an area around the injection site define by a sphere with a radius of 390 μm (which is given simply by the volume equation of the sphere ($V_{inactivated} \approx \frac{4}{3}\pi R_{inactivated}^3$)). 250 Hz digital video was recorded by triggering frames and recording from a Spike2 script and the whisker movements were tracked using a custom written computer software for whisker tracking (Viktor Bahr, adapted from Clack et al. 2012⁶⁰). The whisking was filmed just following the lidocaine injections (i.e. in the few minutes range), where the inactivation by 2% lidocaine injection is largest, and before the cell activity recovers (which happens slowly in the 10-40 min post injection range)⁶⁴. Whisker tracking was done blind to the injected solution (Ringer or lidocaine).

The whisker trace was filtered, and whisking power and whisker set angle was calculated as described above. The ratio of the contralateral whisking power to the ipsilateral whisking power was found to be log-normally distributed (assessed with a Lilliefors test), so we performed log-normal t-tests to assess statistical significance of the ratios.

Vibrissa motor cortex blockade in anaesthetized rats

Rats were anaesthetized and prepared for head-fixation as described above. A square craniotomy was microdrilled above VMC, 0.5 mm - 4.5 mm anterior from bregma and 0.5 mm - 2.0 mm lateral. After dura removal, VMC was superfused with 30 μL blocking solution. The blocking solution was made from 500 μL 1 mM APV (in 0.1 M PBS), 50 μL 100 μM NBQX (in 0.1 M PBS) and 500 μL Ringer's solution. After superfusion of VMC with the blocking solution, the rat was intraperitoneally injected with acepromazine (2 mg/kg). The animal was observed until anaesthesia was light and whisker micromovements were observed (typically ~ 60 mins post first ketamine/xylazine dose). Light anaesthesia was maintained by additional alternating doses of 5% of the initial dose in ketamine/xylazine amount or 5% of the corresponding ketamine dose alone, respectively. As soon as whisker movements were observed, 250 Hz high-speed videos of the whiskers were recorded at 10 min intervals until 160 mins post blocking. In one rat, the time course of the blocking of excitatory transmission in VMC was monitored with a field electrode, and found to be

extinguished in deeper cortical layers of VMC at ~ 100 mins post blocking. Whisker movements were tracked from the 250 Hz video and analyzed as described above.

Vibrissa motor cortex blockade in lightly anaesthetized mice

Mice were anaesthetized and prepared for head-fixation as described above, but given 100 mg/kg ketamine and 15 mg/kg xylazine. A square craniotomy was microdrilled above one hemisphere centered on VMC, 0.8 mm anterior from bregma and 1.0 mm lateral. The mice were supplemented with 0.01 mL acepromazine (2 mg/kg) and a head-fixation post was applied to the skull with cyanoacrylate glue. The mice were head-fixed and kept at body temperature with a heating pad. We waited until the anaesthesia became light and we saw whisker movements begin to emerge. Then VMC activity was blocked by injection of 25 mM muscimol (a GABA_A receptor agonist, Sigma-Aldrich) suspended in Ringer's solution at 10 nL/min (Huber et al. 2012) using a QSI stereotactic injector (Stoelting). In two mice, we only blocked deep VMC, by an injection of 50 nL muscimol solution 900 µm below the dura. In another two mice, we blocked both superficial and deep VMC by injecting 100 nL muscimol solution at 900 µm and another 50 nL muscimol solution at 500 µm. Injection pipettes (Drummond 5µL) were labeled with DiI and the injection sites were confirmed to be in VMC by perfusing the mice and locating the DiI-labeled pipette tracks by fluorescence microscopy. Whisker movements were tracked from the 250 Hz video and analyzed as described above.

Statistical methods

By default, we used non-parametric methods for comparisons: Mann-Whitney U-tests (for un-paired data) or Wilcoxon ranked sum tests (for paired data). If the distributions (or the errors for paired data) were normally distributed as assessed by a Lilliefors test at $p < 0.05$, we used t-tests. All comparisons were two-tailed. Exact p-values are given in the figure legends. After each p-value, we always state, which specific statistical test was used. No statistical methods were used to predetermine sample sizes; however, sample sizes were similar to those generally employed in the field. We did not exclude data points or perform randomization.

A Supplementary Methods Checklist is available.

Data and code availability

Data and scripts will be made available upon request from the corresponding author.

Supplementary Material

Refer to Web version on PubMed Central for supplementary material.

Acknowledgements

We thank Brigitte Geue, Undine Schneeweiß and Juliane Diederichs for technical assistance and Viktor Bahr and Falk Mielke for assistance with programming. We thank Maria Rüsseler for assistance with video tracking and Rajnish P. Rao and Evgeny Bobrov for sharing tracked whisker traces of behaving rats. We thank Sara Helgheim Tawfiq for behavior drawings. We thank Andreea Neukirchner, Edith Chorev, Saikat Ray, Peter Bennett and Ann Clemens for comments on the manuscript. This work was supported by Humboldt-Universität zu Berlin, the

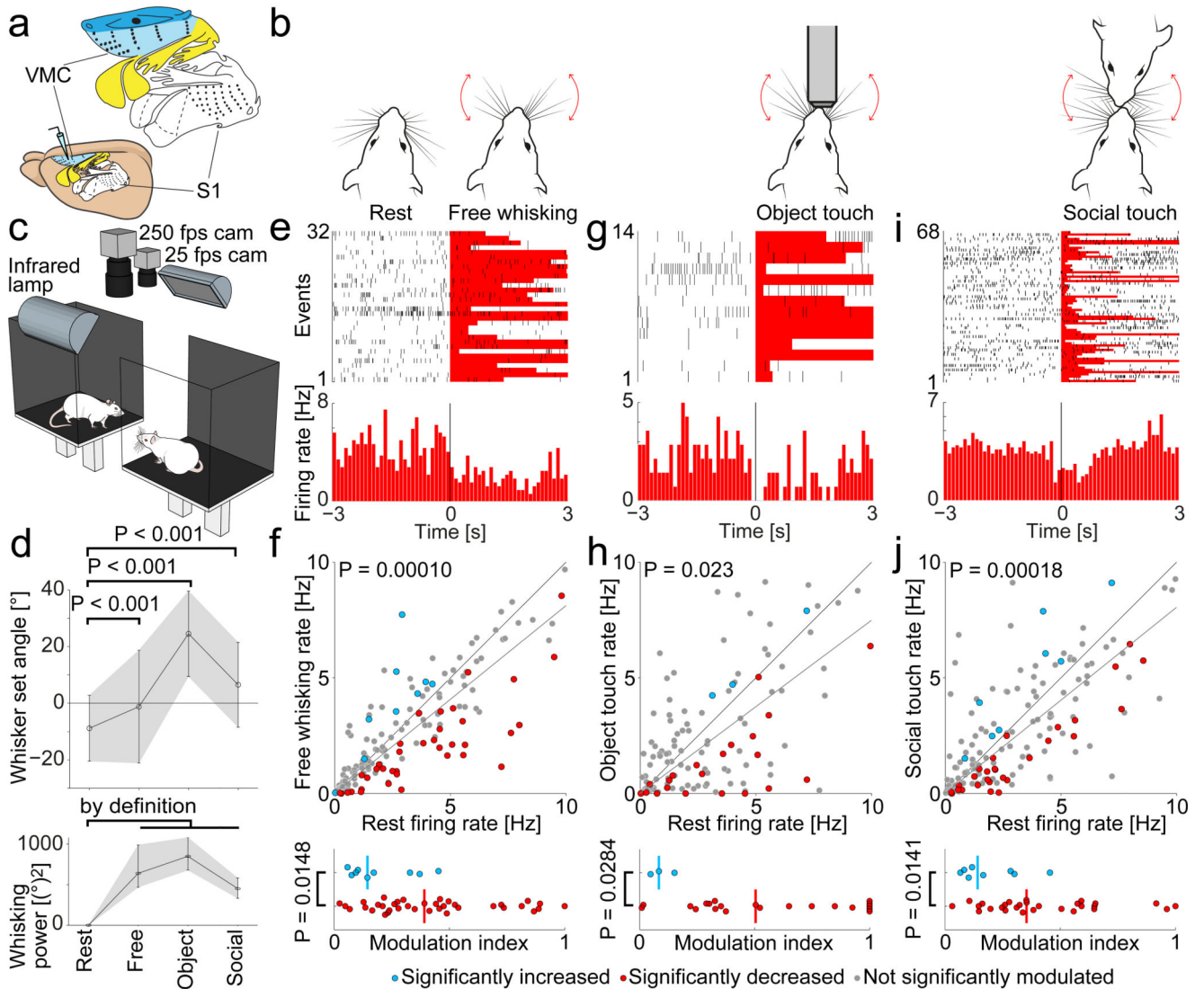
Bernstein Center for Computational Neuroscience Berlin, the German Federal Ministry of Education and Research (BMBF, Förderkennzeichen 01GQ1001A, M.B.) and NeuroCure. M.B. was a recipient of a European Research Council grant and the Gottfried Wilhelm Leibniz Prize.

References

1. Hall RD, Lindholm EP. Organization of motor and somatosensory neocortex in the albino rat. *Brain Res.* 1974; 66:23–38.
2. Gioanni Y, Lamarche M. A reappraisal of rat motor cortex organization by intracortical microstimulation. *Brain Res.* 1985; 344:49–61. [PubMed: 4041868]
3. Haiss F, Schwarz C. Spatial segregation of different modes of movement control in the whisker representation of rat primary motor cortex. *J Neurosci.* 2005; 25:1579–1587. [PubMed: 15703412]
4. Tandon S, Kambi N, Jain N. Overlapping representations of the neck and whiskers in the rat motor cortex revealed by mapping at different anaesthetic depths. *Eur J Neurosci.* 2008; 27:228–237. [PubMed: 18093166]
5. Brecht M, et al. Organization of rat vibrissa motor cortex and adjacent areas according to cytoarchitectonics, microstimulation, and intracellular stimulation of identified cells. *J Comp Neurol.* 2004; 479:360–373. [PubMed: 15514982]
6. Brecht M, Schneider M, Sakmann B, Margrie T. Whisker movements evoked by stimulation of single pyramidal cells in rat motor cortex. 2004; 427
7. Matyas F, et al. Motor control by sensory cortex. *Science.* 2010; 330:1240–1243. [PubMed: 21109671]
8. Neafsey EJ, et al. The organization of the rat motor cortex: A microstimulation mapping study. *Brain Res Rev.* 1986; 11:77–96.
9. Welker WI. Analysis of Sniffing of the Albino Rat. *Behaviour.* 1964; 22:223–244.
10. Kleinfeld D, Ahissar E, Diamond ME. Active sensation: insights from the rodent vibrissa sensorimotor system. *Curr Opin Neurobiol.* 2006; 16:435–444. [PubMed: 16837190]
11. Georgopoulos AP, Schwartz AB, Kettner RE. Neuronal population coding of movement direction. *Science (80-.).* 1986; 233:1416–1419.
12. Lemon R. The output map of the primate motor cortex. *Trends Neurosci.* 1988; 11:501–506. [PubMed: 2469178]
13. Carvell GE, Miller SA, Simons DJ. The relationship of vibrissal motor cortex unit activity to whisking in the awake rat. *Somatosens Mot Res.* 1996; 13:115–127. [PubMed: 8844960]
14. Hill DN, Curtis JC, Moore JD, Kleinfeld D. Primary motor cortex reports efferent control of vibrissa motion on multiple timescales. *Neuron.* 2011; 72:344–356. [PubMed: 22017992]
15. Friedman WA, Zeigler HP, Keller A. Vibrissae motor cortex unit activity during whisking. *J Neurophysiol.* 2012; 107:551–563. [PubMed: 21994257]
16. Gerdjikov TV, Haiss F, Rodriguez-Sierra OE, Schwarz C. Rhythmic whisking area (RW) in rat primary motor cortex: an internal monitor of movement-related signals? *J Neurosci.* 2013; 33:14193–204. [PubMed: 23986253]
17. Asanuma H. Recent developments in the study of the columnar arrangement of neurons within the motor cortex. *Physiol Rev.* 1975; 55:143–156. [PubMed: 806927]
18. Penfield, W, Rasmussen, T. *The Cerebral Cortex of Man.* The Macmillan Company; 1952.
19. Graziano, MSa; Taylor, CSR; Moore, T; Cooke, DF. The cortical control of movement revisited. *Neuron.* 2002; 36:349–362. [PubMed: 12408840]
20. Bobrov E, Wolfe J, Rao RP, Brecht M. The representation of social facial touch in rat barrel cortex. *Curr Biol.* 2014; 24:109–115. [PubMed: 24361064]
21. Wolfe J, Mende C, Brecht M. Social facial touch in rats. *Behav Neurosci.* 2011; 125:900–910. [PubMed: 22122151]
22. Lenschow C, Brecht M. Barrel Cortex Membrane Potential Dynamics in Social Touch. *Neuron.* 2015; 85:718–725. [PubMed: 25640075]
23. Lee E, et al. Enhanced Neuronal Activity in the Medial Prefrontal Cortex during Social Approach Behavior. 2016; 36:6926–6936.

24. Schiemann J, et al. Cellular Mechanisms Underlying Behavioral State-Dependent Bidirectional Modulation of Motor Cortex Output. *Cell Rep.* 2015; doi: 10.1016/j.celrep.2015.04.042
25. Moore JD, et al. Hierarchy of orofacial rhythms revealed through whisking and breathing. *Nature.* 2013; 497:205–210. [PubMed: 23624373]
26. Deschênes M, et al. Inhibition, Not Excitation, Drives Rhythmic Whisking. *Neuron.* 2016; 90:374–387. [PubMed: 27041498]
27. Dörfel J. The musculature of the mystacial vibrissae of the white mouse. *J Anat.* 1982; 135:147–154. [PubMed: 7130049]
28. Haidarliu S, Simony E, Golomb D, Ahissar E. Muscle architecture in the mystacial pad of the rat. *Anat Rec.* 2010; 293:1192–1206.
29. Herfst LJ, Brecht M. Whisker movements evoked by stimulation of single motor neurons in the facial nucleus of the rat. *J Neurophysiol.* 2008; 99:2821–32. [PubMed: 18353915]
30. Huber D, et al. Multiple dynamic representations in the motor cortex during sensorimotor learning. *Nature.* 2012; 484:473–478. [PubMed: 22538608]
31. Semba K, Komisaruk BR. Neural substrates of two different rhythmical vibrissal movements in the rat. *Neuroscience.* 1984; 12:761–774. [PubMed: 6472619]
32. Gao P, Hattox AM, Jones LM, Keller A, Zeigler HP. Whisker motor cortex ablation and whisker movement patterns. *Somatosens Mot Res.* 2003; 20:191–198. [PubMed: 14675958]
33. Kolb B. Functions of the frontal cortex of the rat: a comparative review. *Brain Res.* 1984; 320:65–98. [PubMed: 6440660]
34. Kawai R, et al. Motor Cortex Is Required for Learning but Not for Executing a Motor Skill. *Neuron.* 2015; :800–812. DOI: 10.1016/j.neuron.2015.03.024 [PubMed: 25892304]
35. Stoltz S, Humm JL, Schallert T. Cortical injury impairs contralateral forelimb immobility during swimming: a simple test for loss of inhibitory motor control. *Behav Brain Res.* 1999; 106:127–32. [PubMed: 10595428]
36. Zagha E, Ge X, McCormick DA. Competing Neural Ensembles in Motor Cortex Gate Goal-Directed Motor Output. *Neuron.* 2015; 88:565–577. [PubMed: 26593093]
37. Berg RW, Kleinfeld D. Vibrissa movement elicited by rhythmic electrical microstimulation to motor cortex in the aroused rat mimics exploratory whisking. *J Neurophysiol.* 2003; 90:2950–2963. [PubMed: 12904336]
38. Mikuni N, et al. Evidence for a wide distribution of negative motor areas in the perirolandic cortex. *Clin Neurophysiol.* 2006; 117:33–40. [PubMed: 16314142]
39. Filevich E, Kühn S, Haggard P. Negative motor phenomena in cortical stimulation: Implications for inhibitory control of human action. *Cortex.* 2012; 48:1251–1261. [PubMed: 22658707]
40. Kuypers HGJM. A New Look at the Organization of the Motor System. *Prog Brain Res.* 1982; 57:381–403. [PubMed: 6818612]
41. Grinevich V, Brecht M, Osten P. Monosynaptic pathway from rat vibrissa motor cortex to facial motor neurons revealed by lentivirus-based axonal tracing. *J Neurosci.* 2005; 25:8250–8258. [PubMed: 16148232]
42. Sreenivasan V, Karmakar K, Rijli FM, Petersen CCH. Parallel pathways from motor and somatosensory cortex for controlling whisker movements in mice. *Eur J Neurosci.* 2015; 41:354–367. [PubMed: 25476605]
43. Cheney PD, Fetz EE. Functional classes of primate corticomotoneuronal cells and their relation to active force. *J Neurophysiol.* 1980; 44:773–791. [PubMed: 6253605]
44. Davidson AG, Chan V, O'Dell R, Schieber MH. Rapid changes in throughput from single motor cortex neurons to muscle activity. *Science.* 2007; 318:1934–7. [PubMed: 18096808]
45. Bonini L, Maranesi M, Livi A, Fogassi L, Rizzolatti G. Ventral premotor neurons encoding representations of action during self and others' inaction. *Curr Biol.* 2014; 24:1611–1614. [PubMed: 24998525]
46. Dushanova J, Donoghue J. Neurons in primary motor cortex engaged during action observation. *Eur J Neurosci.* 2010; 31:386–398. [PubMed: 20074212]

47. Vigneswaran G, Philipp R, Lemon RN, Kraskov A. M1 corticospinal mirror neurons and their role in movement suppression during action observation. *Curr Biol*. 2013; 23:236–243. [PubMed: 23290556]
48. Kraskov A, et al. Corticospinal mirror neurons. *Philos Trans R Soc Lond B Biol Sci*. 2014; 369:20130174. [PubMed: 24778371]
49. Schieber MH. Mirror neurons: reflecting on the motor cortex and spinal cord. *Curr Biol*. 2013; 23:R151–2. [PubMed: 23428324]
50. Purves, D, , et al. *Neuroscience*. Sunderland. Sinauer Associates; 2004. doi: 978-087893725
51. Rao RP, Mielke F, Bobrov E, Brecht M. Vocalization–whisking coordination and multisensory integration of social signals in rat auditory cortex. *Elife*. 2014; 3:1–20.
52. Stockwell RG. Localization of the Complex Spectrum: The S Transform. *IEEE Trans Signal Process*. 1996; 44:998–1001.
53. Schmitzer-Torbert N, Jackson J, Henze D, Harris K, Redish aD. Quantitative measures of cluster quality for use in extracellular recordings. *Neuroscience*. 2005; 131:1–11. [PubMed: 15680687]
54. Barthó P, et al. Characterization of neocortical principal cells and interneurons by network interactions and extracellular features. *J Neurophysiol*. 2004; 92:600–608. [PubMed: 15056678]
55. Vigneswaran G, Kraskov A, Lemon R. Large Identified Pyramidal Cells in Macaque Motor and Premotor Cortex Exhibit ‘Thin Spikes’: Implications for Cell Type Classification. 2011; 31:14235–14242.
56. Houweling AR, Doron G, Voigt BC, Herfst LJ, Brecht M. Nanostimulation: manipulation of single neuron activity by juxtacellular current injection. *J Neurophysiol*. 2010; 103:1696–704. [PubMed: 19955285]
57. Pinault D. A novel single-cell staining procedure performed in vivo under electrophysiological control: Morpho-functional features of juxtacellularly labeled thalamic cells and other central neurons with biocytin or Neurobiotin. *J Neurosci Methods*. 1996; 65:113–136. [PubMed: 8740589]
58. Tang Q, Brecht M, Burgalossi A. Juxtacellular recording and morphological identification of single neurons in freely moving rats. *Nat Protoc*. 2014; 9:2369–81. [PubMed: 25211514]
59. Sürmeli G, et al. Molecularly Defined Circuitry Reveals Input-Output Segregation in Deep Layers of the Medial Entorhinal Cortex. *Neuron*. 2015; 88:1040–1053. [PubMed: 26606996]
60. Clack NG, et al. Automated tracking of whiskers in videos of head fixed rodents. *PLoS Comput Biol*. 2012; 8:e1002591. [PubMed: 22792058]
61. MacDonald CJ, Lepage KQ, Eden UT, Eichenbaum H. Hippocampal ‘time cells’ bridge the gap in memory for discontinuous events. *Neuron*. 2011; 71:737–749. [PubMed: 21867888]
62. Tehovnik EJ, Tolias AS, Sultan F, Slocum WM, Logothetis NK. Direct and indirect activation of cortical neurons by electrical microstimulation. *J Neurophysiol*. 2006; 96:512–521. [PubMed: 16835359]
63. Aarts E, Verhage M, Veenliet JV, Dolan CV, van der Sluis S. A solution to dependency: using multilevel analysis to accommodate nested data. *Nat Neurosci*. 2014; 17:491–6. [PubMed: 24671065]
64. Tehovnik EJ, Sommer MA. Effective spread and timecourse of neural inactivation caused by lidocaine injection in monkey cerebral cortex. *J Neurosci Methods*. 1997; 74:17–26. [PubMed: 9210571]



- (e) PSTH of activity of a layer 5 VMC neuron aligned to the onset of free whisking. A significant firing rate-decrease is observed.
- (f) Top: Scatterplot of the firing rate during rest vs. free whisking for VMC layer 5 cells (n=158). The population activity is lower during free whisking ($P = 0.00010$, Wilcoxon signed-rank test, dark grey line indicates slope). Cells with significantly decreased activity during free whisking (red dots), cells with significantly increased activity during free whisking (blue dots), cells not significantly modulated (gray dots). Bottom: Modulation index of significantly rate-increasing (n=9) and rate-decreasing (n=37) cells. Rate-decreasing cells are more strongly modulated ($P = 0.0148$, Mann-Whitney U-test).
- (g) Same as (e) for rest vs. object touch.
- (h) Same as (f) for rest vs. object touch. Population activity is lower during object touch (n=122, $P=0.023$, Wilcoxon signed-rank test, dark grey line indicates slope). Rate-decreasing (n=21) cells are more strongly modulated than rate-increasing (n=3) cells ($P=0.0284$, Mann-Whitney U-test).
- (i) Same as (e) for rest vs. social touch.
- (j) Same as (f) for rest vs. social touch. Population activity is lower during social touch (n=156, $P=0.0018$, Wilcoxon signed-rank test, dark grey line indicates slope). Rate-decreasing (n=28) cells are more strongly modulated than rate-increasing (n=8) cells ($P=0.0141$, Mann-Whitney U-test).

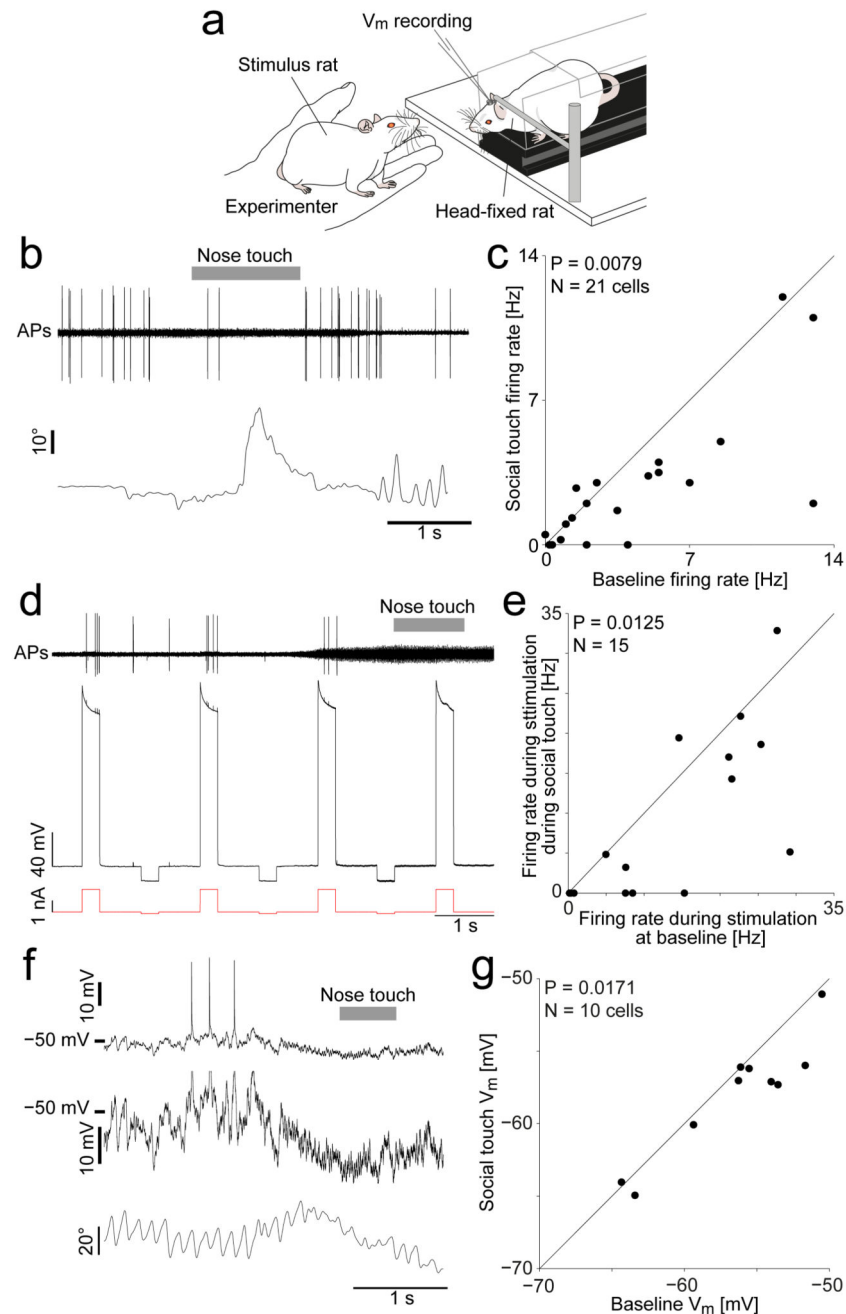


Figure 2. Decreased activity, decreased excitability and hyperpolarization of vibrissa motor cortex during social touch

- (a) VMC recording and nanostimulation in head-fixed rats during staged social touch.
 (b) Top: Example juxtacellular recording in a VMC layer 5 neuron during a social facial interaction, showing a reduction in APs during social touch (nose-to-nose touch indicated by grey bar). Bottom: Angle of contralateral whisker (C2, protraction plotted upwards).
 (c) Scatterplot of firing rate of VMC layer 5 cells (n=21) during social facial touch and baseline (P = 0.0079, Wilcoxon signed-rank test).

(d) Assessment of cell excitability by nanostimulation. Top: Filtered voltage trace of a VMC layer 5 cell. The evoked firing rate during nanostimulation is higher at baseline, than during social touch (indicated by grey bar). Middle: Unfiltered voltage trace. Bottom: Nanostimulation current steps.

(e) Scatterplot of the firing rate of VMC layer 5 cells ($n=15$) when stimulated during social facial touch and baseline ($P = 0.0125$, Wilcoxon signed-rank test).

(f) Top: Example whole-cell patch clamp recording from a VMC layer 5 cell showing a hyperpolarization of the membrane potential during social facial touch (duration of nose-to-nose touch indicated by grey bar). Middle: Zoom of the above trace (Spikes clipped). Bottom: Angle of contralateral whisker (C2).

(g) Scatterplot of the membrane potential (V_m) of VMC layer 5 cells ($n=10$) during social facial touch and baseline ($P = 0.0171$, $t(9)=2.90$, paired t-test).

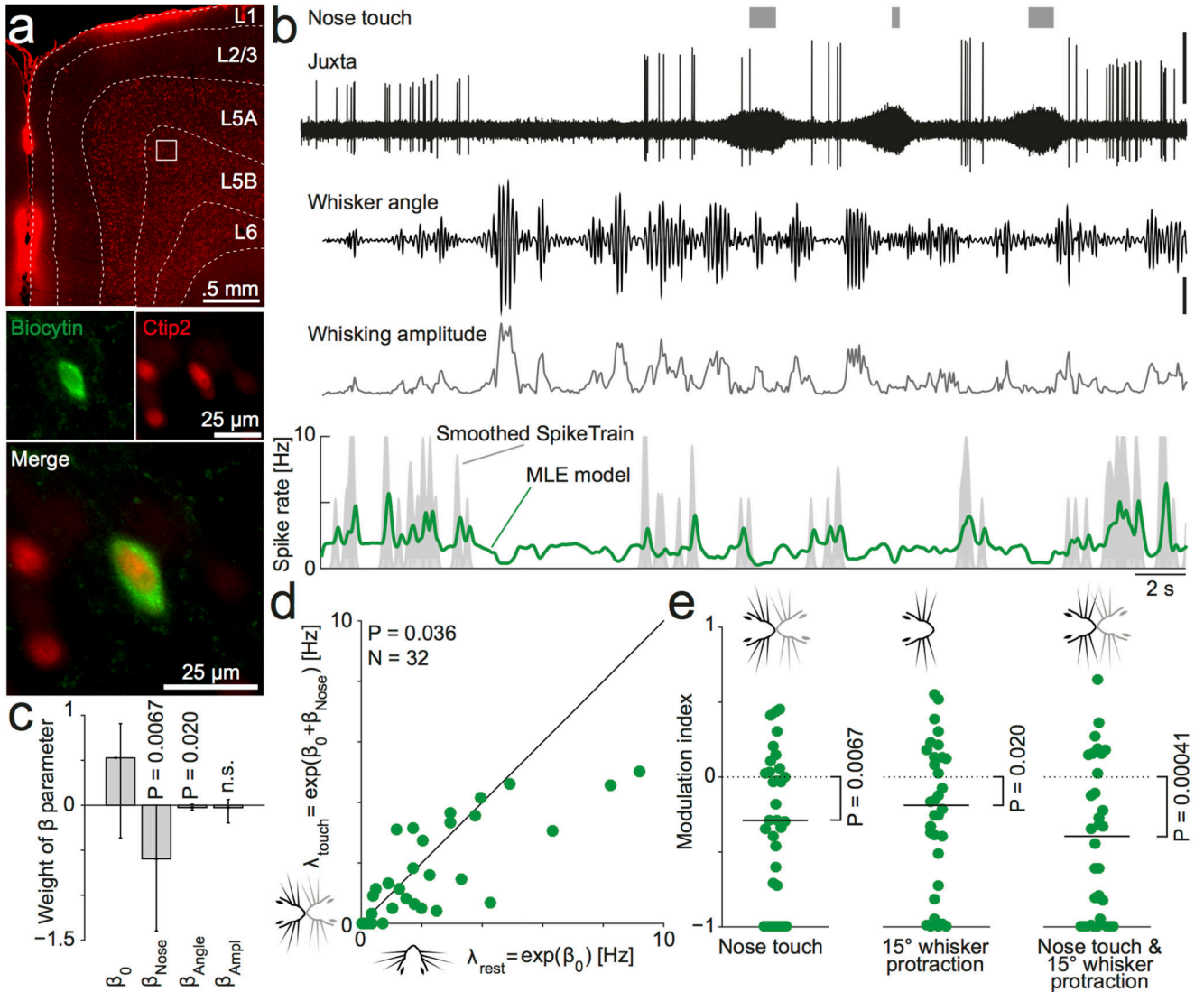


Figure 3. Vibrissa motor cortex activity is additively suppressed by both nose-to-nose touch and whisker protraction.

(a) Example soma of a juxtacellularly labeled neuron in layer 5B of VMC. Top: Overview of coronal section of the VMC showing a wide layer 5, which contains a large fraction of Ctip2-positive, putative thick-tufted pyramidal tract (PT-type) neurons (Red channel = Ctip2, white lines indicate layer boundaries traced on brightfield image, white square indicates location of labeled soma: 1.25mm deep, 1.21 mm medial, uncorrected for shrinkage). Bottom: Close up image of the juxtacellularly recorded soma (labeled by biocytin filling, green channel), which is Ctip2-positive (red channel).

(b) Example recorded data and fitted model from the neuron shown in (a). The top traces show the occurrence of nose-to-nose touches (grey bars), the juxtacellular recording trace with spikes (high-pass filtered at 300 Hz, top trace, scale bar = 1 mV) and the whisker angle and whisking amplitude (tracked by high-speed videography, scale bar = 5°). Below we show the estimate of the instantaneous firing rate of the best fitted model ('MLE model',

green line, smoothed with a Gaussian with $\sigma = 75$ ms for plotting, real model is run with 1-ms bins) plotted on top of an estimate of the observed firing rate ('Smoothed SpikeTrain', grey area, calculated by convolving the spike train with a Gaussian with $\sigma = 75$ ms, clipped at 10 Hz for plotting). This cell was suppressed by nose touch, whisker protraction and by increased whisking amplitude (maximum likelihood estimates: $\beta_0 = 0.68$, $\beta_{Nose} = -1.40$, $\beta_{Angle} = -0.06$ ($^\circ$)⁻¹, $\beta_{Ampl} = -0.20$ ($^\circ$)⁻¹)

(c) Across the population (n=32 cells), VMC activity is significantly suppressed by nose-to-nose touch (median $\beta_{Nose} < 0$, $P=0.0067$, Wilcoxon signed-rank test) and whisker protraction (median $\beta_{Angle} < 0$, $P=0.02$, Wilcoxon signed-rank test), but not significantly modulated by changes in whisking amplitude ($P=0.2$). Bars indicate median β , error bars indicate 95% confidence interval of the median.

(d) Evaluating the MLE model to estimate the firing rate at rest $\lambda_{rest} = \exp(\beta_0)$ and during nose touch $\lambda_{touch} = \exp(\beta_0 + \beta_{Nose})$ recapitulates the finding from Fig 2c: nose-to-nose touch suppresses VMC activity (n=32, $t(31)=2.2$, $P=0.036$, paired t-test).

(e) Evaluation of the fitted model during three behavioral states demonstrate, that the suppression due to nose touch and whisker protraction is additive: nose touch in the absence of whisker protraction (left), 15° whisker protraction in absence of nose touch (middle) and nose touch coinciding with 15° whisker protraction (right) all suppress VMC activity compared to rest.

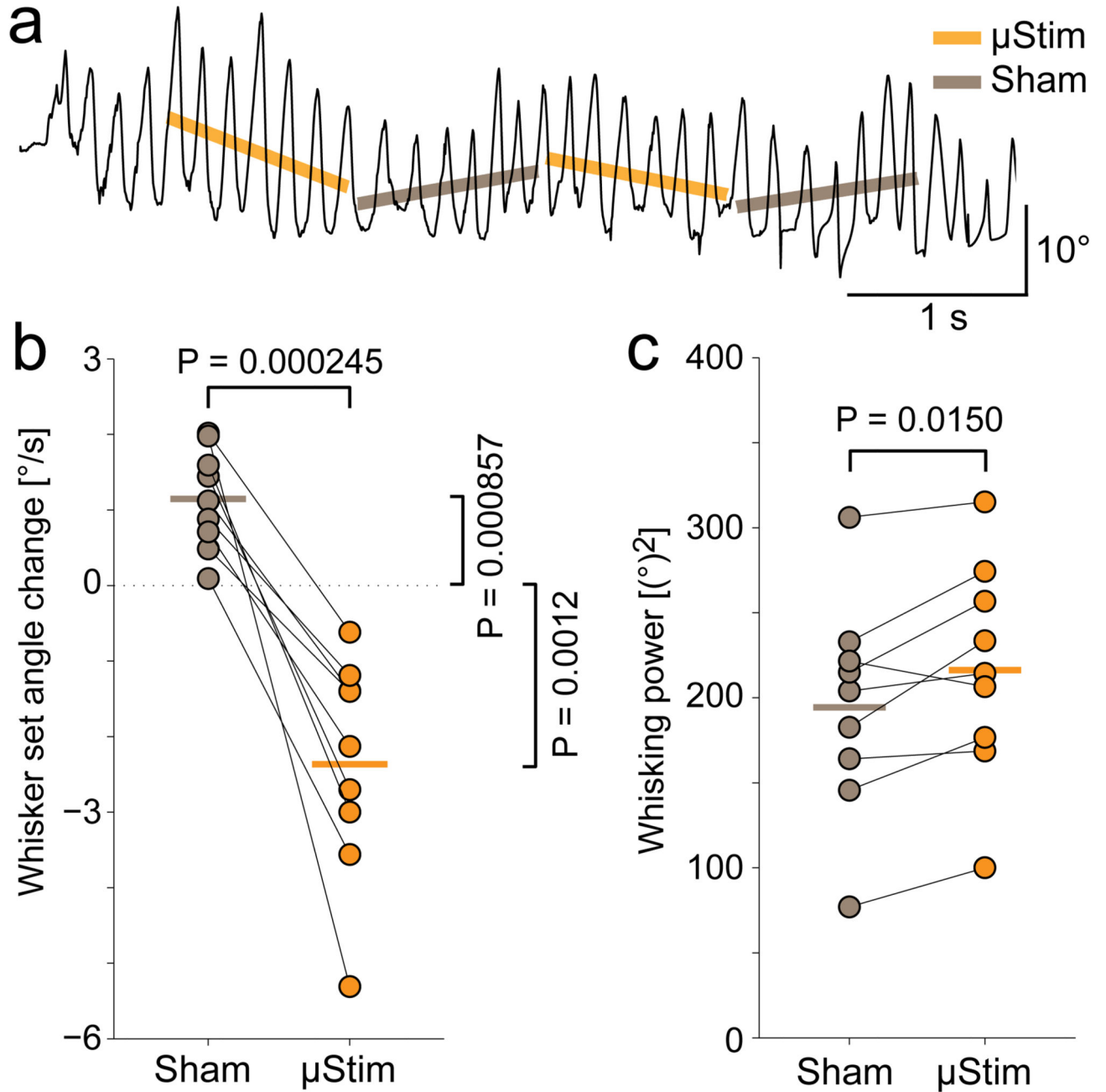


Figure 4. Unilateral microstimulation of vibrissa motor cortex in awake rats leads to contralateral whisker retraction.

(a) Trace of rat whisking during a microstimulation experiment (C2, protraction plotted upwards). Stimulation is delivered in 1 s long pulse trains (“ μ Stim”, slope denoted by orange line) alternating with 1 s pauses (“Sham”, slope denoted by grey line).

(b) Comparison of whisker set angle change during periods of sham stimulation (grey dots) and microstimulation (orange dots, vertical lines indicate means) $n=9$, $t(8)=6.17$, $P = 0.0002$, paired t-test).

(c) Same as (b) for whisking power ($n=9$, $t(8)=-3.08$, $P = 0.0150$, paired t-test).

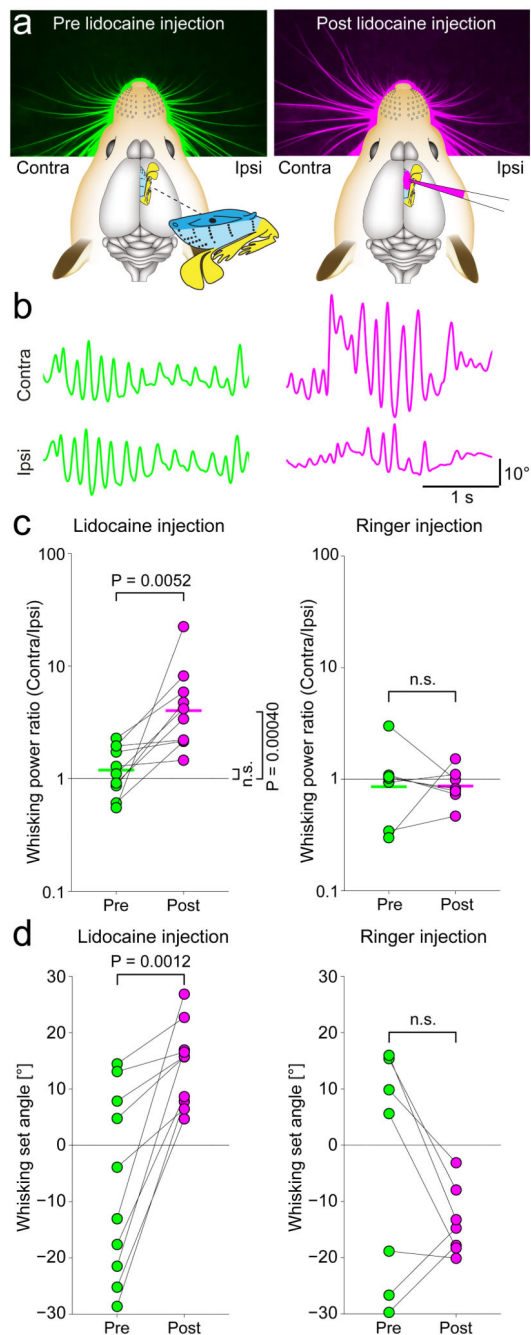


Figure 5. Unilateral blockade of vibrissa motor cortex increases contralateral whisker movement and protraction.

(a) Left: Rat whisker set angles at rest before unilateral lidocaine injection (green color). Right: whisker set angles after unilateral lidocaine injection (pink color) in deep layers of VMC. Lidocaine injection leads to a protraction of the contralateral whiskers.

(b) Ipsilateral and contralateral whisker traces prior to (green color) and after (pink color) lidocaine injection (protraction plotted upwards). Prior to injection, whisking is similar on both sides, after injection the contralateral whiskers move more.

(c) Left: bilaterally symmetric whisking during baseline (contralateral and ipsilateral whisking power ratio ≈ 1 , green dots) changes to a predominance of contralateral whisking after lidocaine injection into VMC deep layers (pink dots, $n=10$, $t(9)=-3.66$, $P = 0.0052$, paired t-test, lines indicate means). Right: Control injections of ringer have no such effect, ($n=7$, $t(6)=0.04$, $P = 0.97$, paired t-test).

(d) Same as (c) for whisking set angle. Lidocaine injection results in contralateral protraction (Ringer: $n=7$, $t(6)=1.46$, $P = 0.19$, Lidocaine: $n=10$, $t(9)=-4.66$, $P = 0.0012$, paired t-tests).